

Measurement of Prompt Charm Meson Production Cross Sections in $p\bar{p}$ Collisions at $\sqrt{s} = 1.96 \text{ TeV}$

D. Acosta,¹⁴ T. Affolder,⁷ M.H. Ahn,²⁵ T. Akimoto,⁵² M.G. Albrow,¹³ D. Ambrose,⁴⁰
D. Amidei,³⁰ A. Anastassov,⁴⁷ K. Anikeev,²⁹ A. Annovi,⁴¹ J. Antos,¹ M. Aoki,⁵²
G. Apollinari,¹³ J-F. Arguin,⁵⁰ T. Arisawa,⁵⁴ A. Artikov,¹¹ T. Asakawa,⁵² W. Ashmanskas,²
A. Attal,⁶ F. Azfar,³⁸ P. Azzi-Bacchetta,³⁹ N. Bacchetta,³⁹ H. Bachacou,²⁶ W. Badgett,¹³
S. Bailey,¹⁸ A. Barbaro-Galtieri,²⁶ G. Barker,²³ V.E. Barnes,⁴³ B.A. Barnett,²²
S. Baroiant,⁵ M. Barone,¹⁵ G. Bauer,²⁹ F. Bedeschi,⁴¹ S. Behari,²² S. Belforte,⁵¹
W.H. Bell,¹⁷ G. Bellettini,⁴¹ J. Bellinger,⁵⁵ D. Benjamin,¹² A. Beretvas,¹³ A. Bhatti,⁴⁵
M. Binkley,¹³ D. Bisello,³⁹ M. Bishai,¹³ R.E. Blair,² C. Blocker,⁴ K. Bloom,³⁰
B. Blumenfeld,²² A. Bocci,⁴⁵ A. Bodek,⁴⁴ G. Bolla,⁴³ A. Bolshov,²⁹ P.S.L. Booth,²⁷
D. Bortoletto,⁴³ J. Boudreau,⁴² S. Bourov,¹³ C. Bromberg,³¹ M. Brozovic,¹²
E. Brubaker,²⁶ J. Budagov,¹¹ H.S. Budd,⁴⁴ K. Burkett,¹⁸ G. Busetto,³⁹ P. Bussey,¹⁷
K.L. Byrum,² S. Cabrera,¹² P. Calafiura,²⁶ M. Campanelli,¹⁶ M. Campbell,³⁰
A. Canepa,⁴³ D. Carlsmith,⁵⁵ S. Carron,¹² R. Carosi,⁴¹ M. Casarsa,⁵¹ W. Caskey,⁵
A. Castro,³ P. Catastini,⁴¹ D. Cauz,⁵¹ A. Cerri,²⁶ C. Cerri,⁴¹ L. Cerrito,²¹ J. Chapman,³⁰
C. Chen,⁴⁰ Y.C. Chen,¹ M. Chertok,⁵ G. Chiarelli,⁴¹ G. Chlachidze,¹¹ F. Chlebana,¹³
K. Cho,²⁵ D. Chokheli,¹¹ M.L. Chu,¹ J.Y. Chung,³⁵ W-H. Chung,⁵⁵ Y.S. Chung,⁴⁴
C.I. Ciobanu,²¹ M.A. Ciocci,⁴¹ A.G. Clark,¹⁶ M.N. Coca,⁴⁴ A. Connolly,²⁶ M.E. Convery,⁴⁵
J. Conway,⁴⁷ M. Cordelli,¹⁵ G. Cortiana,³⁹ J. Cranshaw,⁴⁹ R. Culbertson,¹³ C. Currat,²⁶
D. Cyr,⁵⁵ D. Dagenhart,⁴ S. DaRonco,³⁹ S. D'Auria,¹⁷ P. de Barbaro,⁴⁴ S. De Cecco,⁴⁶
S. Dell'Agnello,¹⁵ M. Dell'Orso,⁴¹ S. Demers,⁴⁴ L. Demortier,⁴⁵ M. Deninno,³
D. De Pedis,⁴⁶ P.F. Derwent,¹³ C. Dionisi,⁴⁶ J.R. Dittmann,¹³ P. Doksus,²¹
A. Dominguez,²⁶ S. Donati,⁴¹ M. D'Onofrio,¹⁶ T. Dorigo,³⁹ V. Drollinger,³³ K. Ebina,⁵⁴
N. Eddy,²¹ R. Ely,²⁶ R. Erbacher,¹³ M. Erdmann,²³ D. Errede,²¹ S. Errede,²¹ R. Eusebi,⁴⁴
H-C. Fang,²⁶ S. Farrington,¹⁷ I. Fedorko,⁴¹ R.G. Feild,⁵⁶ M. Feindt,²³ J.P. Fernandez,⁴³
C. Ferretti,³⁰ R.D. Field,¹⁴ I. Fiori,⁴¹ G. Flanagan,³¹ B. Flaugh,¹³ L.R. Flores-Castillo,⁴²
A. Foland,¹⁸ S. Forrester,⁵ G.W. Foster,¹³ M. Franklin,¹⁸ H. Frisch,¹⁰ Y. Fujii,²⁴ I. Furic,²⁹
A. Gallas,³⁴ M. Gallinaro,⁴⁵ J. Galyardt,⁹ M. Garcia-Sciveres,²⁶ A.F. Garfinkel,⁴³ C. Gay,⁵⁶
H. Gerberich,¹² E. Gerchtein,⁹ D.W. Gerdes,³⁰ S. Giagu,⁴⁶ P. Giannetti,⁴¹ A. Gibson,²⁶

K. Gibson,⁹ C. Ginsburg,⁵⁵ K. Giolo,⁴³ M. Giordani,⁵ G. Giurgiu,⁹ V. Glagolev,¹¹
D. Glenzinski,¹³ M. Gold,³³ N. Goldschmidt,³⁰ D. Goldstein,⁶ J. Goldstein,¹³
G. Gomez,⁸ G. Gomez-Ceballos,²⁹ M. Goncharov,⁴⁸ I. Gorelov,³³ A.T. Goshaw,¹²
Y. Gotra,⁴² K. Goulianatos,⁴⁵ A. Gresele,³ G. Grim,⁵ C. Grossos-Pilcher,¹⁰ M. Guenther,⁴³
J. Guimaraes da Costa,¹⁸ C. Haber,²⁶ K. Hahn,⁴⁰ S.R. Hahn,¹³ E. Halkiadakis,⁴⁴ C. Hall,¹⁸
R. Handler,⁵⁵ F. Happacher,¹⁵ K. Hara,⁵² M. Hare,⁵³ R.F. Harr,³⁰ R.M. Harris,¹³
F. Hartmann,²³ K. Hatakeyama,⁴⁵ J. Hauser,⁶ C. Hays,¹² E. Heider,⁵³ B. Heinemann,²⁷
J. Heinrich,⁴⁰ M. Hennecke,²³ M. Herndon,²² C. Hill,⁷ D. Hirschbuehl,²³ A. Hocker,⁴⁴
K.D. Hoffman,¹⁰ A. Holloway,¹⁸ S. Hou,¹ M.A. Houlden,²⁷ B.T. Huffman,³⁸ R.E. Hughes,³⁵
J. Huston,³¹ K. Ikado,⁵⁴ J. Incandela,⁷ G. Introzzi,⁴¹ M. Iori,⁴⁶ Y. Ishizawa,⁵²
C. Issever,⁷ A. Ivanov,⁴⁴ Y. Iwata,²⁰ B. Iyutin,²⁹ E. James,³⁰ D. Jang,⁴⁷ J. Jarrell,³³
D. Jeans,⁴⁶ H. Jensen,¹³ M. Jones,⁴⁰ S.Y. Jun,⁹ T. Junk,²¹ T. Kamon,⁴⁸ J. Kang,³⁰
M. Karagoz Unel,³⁴ P.E. Karchin,³⁰ S. Kartal,¹³ Y. Kato,³⁷ Y. Kemp,²³ R. Kephart,¹³
U. Kerzel,²³ D. Khazins,¹² V. Khotilovich,⁴⁸ B. Kilminster,⁴⁴ B.J. Kim,²⁵ D.H. Kim,²⁵
H.S. Kim,²¹ J.E. Kim,²⁵ M.J. Kim,⁹ M.S. Kim,²⁵ S.B. Kim,²⁵ S.H. Kim,⁵² T.H. Kim,²⁹
Y.K. Kim,¹⁰ B.T. King,²⁷ M. Kirby,¹² M. Kirk,⁴ L. Kirsch,⁴ S. Klimenko,¹⁴ B. Knuteson,¹⁰
H. Kobayashi,⁵² P. Koehn,³⁵ K. Kondo,⁵⁴ J. Konigsberg,¹⁴ K. Kordas,⁵⁰ A. Korn,²⁹
A. Korytov,¹⁴ K. Kotelnikov,³² A.V. Kotwal,¹² A. Kovalev,⁴⁰ J. Kraus,²¹ I. Kravchenko,²⁹
A. Kreymer,¹³ J. Kroll,⁴⁰ M. Kruse,¹² V. Krutelyov,⁴⁸ S.E. Kuhlmann,² N. Kuznetsova,¹³
A.T. Laasanen,⁴³ S. Lai,⁵⁰ S. Lami,⁴⁵ S. Lammel,¹³ J. Lancaster,¹² M. Lancaster,²⁸
R. Lander,⁵ K. Lannon,²¹ A. Lath,⁴⁷ G. Latino,³³ R. Lauhakangas,¹⁹ I. Lazzizzera,³⁹
Y. Le,²² C. Lecci,²³ T. LeCompte,² J. Lee,²⁵ J. Lee,⁴⁴ S.W. Lee,⁴⁸ N. Leonardo,²⁹
S. Leone,⁴¹ J.D. Lewis,¹³ K. Li,⁵⁶ C.S. Lin,¹³ M. Lindgren,⁶ T.M. Liss,²¹ D.O. Litvintsev,¹³
T. Liu,¹³ Y. Liu,¹⁶ N.S. Lockyer,⁴⁰ A. Loginov,³² J. Loken,³⁸ M. Loretta,³⁹ P. Loverre,⁴⁶
D. Lucchesi,³⁹ P. Lukens,¹³ L. Lyons,³⁸ J. Lys,²⁶ D. MacQueen,⁵⁰ R. Madrak,¹⁸
K. Maeshima,¹³ P. Maksimovic,²² L. Malferrari,³ G. Manca,³⁸ R. Marginean,³⁵ A. Martin,⁵⁶
M. Martin,²² V. Martin,³⁴ M. Martinez,¹³ T. Maruyama,¹⁰ H. Matsunaga,⁵² M. Mattson,³⁰
P. Mazzanti,³ K.S. McFarland,⁴⁴ D. McGivern,²⁸ P.M. McIntyre,⁴⁸ P. McNamara,⁴⁷
R. McNulty,²⁷ S. Menzemer,²³ A. Menzione,⁴¹ P. Merkel,¹³ C. Mesropian,⁴⁵ A. Messina,⁴⁶
A. Meyer,¹³ T. Miao,¹³ L. Miller,¹⁸ R. Miller,³¹ J.S. Miller,³⁰ R. Miquel,²⁶ S. Miscetti,¹⁵

M. Mishina,¹³ G. Mitselmakher,¹⁴ A. Miyamoto,²⁴ Y. Miyazaki,³⁷ N. Moggi,³ R. Moore,¹³
M. Morello,⁴¹ T. Moulik,⁴³ A. Mukherjee,¹³ M. Mulhearn,²⁹ T. Muller,²³ R. Mumford,²²
A. Munar,⁴⁰ P. Murat,¹³ S. Murgia,³¹ J. Nachtman,¹³ S. Nahn,⁵⁶ I. Nakamura,⁴⁰
I. Nakano,³⁶ A. Napier,⁵³ R. Napora,²² V. Necula,¹⁴ F. Niell,³⁰ J. Nielsen,²⁶ C. Nelson,¹³
T. Nelson,¹³ C. Neu,³⁵ M.S. Neubauer,²⁹ C. Newman-Holmes,¹³ A-S. Nicollerat,¹⁶
T. Nigmanov,⁴² H. Niu,⁴ L. Nodulman,² K. Oesterberg,¹⁹ T. Ogawa,⁵⁴ S. Oh,¹² Y.D. Oh,²⁵
T. Ohsugi,²⁰ R. Oishi,⁵² T. Okusawa,³⁷ R. Oldeman,⁴⁰ R. Orava,¹⁹ W. Orejudos,²⁶
C. Pagliarone,⁴¹ F. Palmonari,⁴¹ R. Paoletti,⁴¹ V. Papadimitriou,⁴⁹ D. Partos,⁴
S. Pashapour,⁵⁰ J. Patrick,¹³ G. Pauletta,⁵¹ M. Paulini,⁹ T. Pauly,³⁸ C. Paus,²⁹ D. Pellett,⁵
A. Penzo,⁵¹ T.J. Phillips,¹² G. Piacentino,⁴¹ J. Piedra,⁸ K.T. Pitts,²¹ A. Pompoš,⁴³
L. Pondrom,⁵⁵ G. Pope,⁴² O. Poukhov,¹¹ F. Prakoshyn,¹¹ T. Pratt,²⁷ A. Pronko,¹⁴
J. Proudfoot,² F. Ptahos,¹⁵ G. Punzi,⁴¹ J. Rademacker,³⁸ A. Rakitine,²⁹ S. Rappoccio,¹⁸
F. Ratnikov,⁴⁷ H. Ray,³⁰ A. Reichold,³⁸ V. Rekovic,³³ P. Renton,³⁸ M. Rescigno,⁴⁶
F. Rimondi,³ K. Rinnert,²³ L. Ristori,⁴¹ M. Riveline,⁵⁰ W.J. Robertson,¹² A. Robson,³⁸
T. Rodrigo,⁸ S. Rolli,⁵³ L. Rosenson,²⁹ R. Roser,¹³ R. Rossin,³⁹ C. Rott,⁴³ J. Russ,⁹
A. Ruiz,⁸ D. Ryan,⁵³ H. Saarikko,¹⁹ A. Safonov,⁵ R. St. Denis,¹⁷ W.K. Sakumoto,⁴⁴
D. Saltzberg,⁶ C. Sanchez,³⁵ A. Sansoni,¹⁵ L. Santi,⁵¹ S. Sarkar,⁴⁶ K. Sato,⁵² P. Savard,⁵⁰
A. Savoy-Navarro,¹³ P. Schemitz,²³ P. Schlabach,¹³ E.E. Schmidt,¹³ M.P. Schmidt,⁵⁶
M. Schmitt,³⁴ G. Schofield,⁵ L. Scodellaro,³⁹ A. Scribano,⁴¹ F. Scuri,⁴¹ A. Sedov,⁴³
S. Seidel,³³ Y. Seiya,⁵² F. Semeria,³ L. Sexton-Kennedy,¹³ I. Sfiligoi,¹⁵ M.D. Shapiro,²⁶
T. Shears,²⁷ P.F. Shepard,⁴² M. Shimojima,⁵² M. Shochet,¹⁰ Y. Shon,⁵⁵ A. Sidoti,⁴¹
M. Siket,¹ A. Sill,⁴⁹ P. Sinervo,⁵⁰ A. Sisakyan,¹¹ A. Skiba,²³ A.J. Slaughter,¹³
K. Sliwa,⁵³ J.R. Smith,⁵ F.D. Snider,¹³ R. Snihur,²⁸ S.V. Somalwar,⁴⁷ J. Spalding,¹³
M. Spezziga,⁴⁹ L. Spiegel,¹³ F. Spinella,⁴¹ M. Spiropulu,¹⁰ H. Stadie,²³ B. Stelzer,⁵⁰
O. Stelzer-Chilton,⁵⁰ J. Strologas,²¹ D. Stuart,⁷ A. Sukhanov,¹⁴ K. Sumorok,²⁹ H. Sun,⁵³
T. Suzuki,⁵² A. Taffard,²¹ S.F. Takach,³⁰ H. Takano,⁵² R. Takashima,²⁰ Y. Takeuchi,⁵²
K. Takikawa,⁵² P. Tamburello,¹² M. Tanaka,² R. Tanaka,³⁶ B. Tannenbaum,⁶
N. Tanimoto,³⁶ S. Tapprogge,¹⁹ M. Tecchio,³⁰ P.K. Teng,¹ K. Terashi,⁴⁵ R.J. Tesarek,¹³
S. Tether,²⁹ J. Thom,¹³ A.S. Thompson,¹⁷ E. Thomson,³⁵ R. Thurman-Keup,² P. Tipton,⁴⁴
V. Tiwari,⁹ S. Tkaczyk,¹³ D. Toback,⁴⁸ K. Tollefson,³¹ D. Tonelli,⁴¹ M. Tönnesmann,³¹

S. Torre,⁴¹ D. Torretta,¹³ W. Trischuk,⁵⁰ J. Tseng,²⁹ R. Tsuchiya,⁵⁴ S. Tsuno,⁵²
 D. Tsybychev,¹⁴ N. Turini,⁴¹ M. Turner,²⁷ F. Ukegawa,⁵² T. Unverhau,¹⁷ S. Uozumi,⁵²
 D. Usynin,⁴⁰ L. Vacavant,²⁶ T. Vaiciulis,⁴⁴ A. Varganov,³⁰ E. Vataga,⁴¹ S. Vejcik III,¹³
 G. Velev,¹³ G. Veramendi,²⁶ T. Vickey,²¹ R. Vidal,¹³ I. Vila,⁸ R. Vilar,⁸ I. Volobouev,²⁶
 M. von der Mey,⁶ R. G. Wagner,² R. L. Wagner,¹³ W. Wagner,²³ N. Wallace,⁴⁷ T. Walter,²³
 Z. Wan,⁴⁷ M.J. Wang,¹ S.M. Wang,¹⁴ B. Ward,¹⁷ S. Waschke,¹⁷ D. Waters,²⁸ T. Watts,⁴⁷
 M. Weber,²⁶ W. Wester,¹³ B. Whitehouse,⁵³ A.B. Wicklund,² E. Wicklund,¹³ T. Wilkes,⁵
 H.H. Williams,⁴⁰ P. Wilson,¹³ B.L. Winer,³⁵ P. Wittich,⁴⁰ S. Wolbers,¹³ M. Wolter,⁵³
 M. Worcester,⁶ S. Worm,⁴⁷ T. Wright,³⁰ X. Wu,¹⁶ F. Würthwein,²⁹ A. Wyatt,²⁸ A. Yagil,¹³
 T. Yamashita,³⁶ K. Yamamoto,³⁷ U.K. Yang,¹⁰ W. Yao,²⁶ G.P. Yeh,¹³ K. Yi,²²
 J. Yoh,¹³ P. Yoon,⁴⁴ K. Yorita,⁵⁴ T. Yoshida,³⁷ I. Yu,²⁵ S. Yu,⁴⁰ Z. Yu,⁵⁶ J.C. Yun,¹³
 L. Zanello,⁴⁶ A. Zanetti,⁵¹ I. Zaw,¹⁸ F. Zetti,⁴¹ J. Zhou,⁴⁷ A. Zsenei,¹⁶ and S. Zucchelli³

¹*Institute of Physics, Academia Sinica,*

Taipei, Taiwan 11529, Republic of China

²*Argonne National Laboratory, Argonne, Illinois 60439*

³*Istituto Nazionale di Fisica Nucleare,*

University of Bologna, I-40127 Bologna, Italy

⁴*Brandeis University, Waltham, Massachusetts 02254*

⁵*University of California at Davis, Davis, California 95616*

⁶*University of California at Los Angeles, Los Angeles, California 90024*

⁷*University of California at Santa Barbara, Santa Barbara, California 93106*

⁸*Instituto de Fisica de Cantabria, CSIC-University of Cantabria, 39005 Santander, Spain*

⁹*Carnegie Mellon University, Pittsburgh, Pennsylvania 15213*

¹⁰*Enrico Fermi Institute, University of Chicago, Chicago, Illinois 60637*

¹¹*Joint Institute for Nuclear Research, RU-141980 Dubna, Russia*

¹²*Duke University, Durham, North Carolina 27708*

¹³*Fermi National Accelerator Laboratory, Batavia, Illinois 60510*

¹⁴*University of Florida, Gainesville, Florida 32611*

¹⁵*Laboratori Nazionali di Frascati, Istituto Nazionale di Fisica Nucleare, I-00044 Frascati, Italy*

¹⁶*University of Geneva, CH-1211 Geneva 4, Switzerland*

¹⁷Glasgow University, Glasgow G12 8QQ, United Kingdom

¹⁸Harvard University, Cambridge, Massachusetts 02138

¹⁹The Helsinki Group: Helsinki Institute of Physics; and Division of High Energy Physics,
Department of Physical Sciences, University of Helsinki, FIN-00014 Helsinki, Finland

²⁰Hiroshima University, Higashi-Hiroshima 724, Japan

²¹University of Illinois, Urbana, Illinois 61801

²²The Johns Hopkins University, Baltimore, Maryland 21218

²³Institut für Experimentelle Kernphysik,

Universität Karlsruhe, 76128 Karlsruhe, Germany

²⁴High Energy Accelerator Research Organization (KEK), Tsukuba, Ibaraki 305, Japan

²⁵Center for High Energy Physics: Kyungpook National University,

Taegu 702-701; Seoul National University,

Seoul 151-742; and SungKyunKwan University, Suwon 440-746; Korea

²⁶Ernest Orlando Lawrence Berkeley National Laboratory, Berkeley, California 94720

²⁷University of Liverpool, Liverpool L69 7ZE, United Kingdom

²⁸University College London, London WC1E 6BT, United Kingdom

²⁹Massachusetts Institute of Technology, Cambridge, Massachusetts 02139

³⁰University of Michigan, Ann Arbor, Michigan 48109

³¹Michigan State University, East Lansing, Michigan 48824

³²Institution for Theoretical and Experimental Physics, ITEP, Moscow 117259, Russia

³³University of New Mexico, Albuquerque, New Mexico 87131

³⁴Northwestern University, Evanston, Illinois 60208

³⁵The Ohio State University, Columbus, Ohio 43210

³⁶Okayama University, Okayama 700-8530, Japan

³⁷Osaka City University, Osaka 588, Japan

³⁸University of Oxford, Oxford OX1 3RH, United Kingdom

³⁹Università di Padova, Istituto Nazionale di Fisica Nucleare,

Sezione di Padova-Trento, I-35131 Padova, Italy

⁴⁰University of Pennsylvania, Philadelphia, Pennsylvania 19104

⁴¹Istituto Nazionale di Fisica Nucleare,

University and Scuola Normale Superiore of Pisa, I-56100 Pisa, Italy

⁴²*University of Pittsburgh, Pittsburgh, Pennsylvania 15260*

⁴³*Purdue University, West Lafayette, Indiana 47907*

⁴⁴*University of Rochester, Rochester, New York 14627*

⁴⁵*The Rockefeller University, New York, New York 10021*

⁴⁶*Instituto Nazionale de Fisica Nucleare, Sezione di Roma,
University di Roma I, “La Sapienza,” I-00185 Roma, Italy*

⁴⁷*Rutgers University, Piscataway, New Jersey 08855*

⁴⁸*Texas A&M University, College Station, Texas 77843*

⁴⁹*Texas Tech University, Lubbock, Texas 79409*

⁵⁰*Institute of Particle Physics, University of Toronto, Toronto M5S 1A7, Canada*

⁵¹*Istituto Nazionale di Fisica Nucleare,
Universities of Trieste and Udine, Italy*

⁵²*University of Tsukuba, Tsukuba, Ibaraki 305, Japan*

⁵³*Tufts University, Medford, Massachusetts 02155*

⁵⁴*Waseda University, Tokyo 169, Japan*

⁵⁵*University of Wisconsin, Madison, Wisconsin 53706*

⁵⁶*Yale University, New Haven, Connecticut 06520*

We report on measurements of differential cross sections $d\sigma/dp_T$ for prompt charm meson production in $p\bar{p}$ collisions at $\sqrt{s} = 1.96$ TeV using $5.8 \pm 0.3 \text{ pb}^{-1}$ of data from the CDF II detector at the Fermilab Tevatron. The data are collected with a new trigger that is sensitive to the long lifetime of hadrons containing heavy flavor. The charm meson cross sections are measured in the central rapidity region $|y| \leq 1$ in four fully reconstructed decay modes: $D^0 \rightarrow K^-\pi^+$, $D^{*+} \rightarrow D^0\pi^+$, $D^+ \rightarrow K^-\pi^+\pi^+$, $D_s^+ \rightarrow \phi\pi^+$, and their charge conjugates. The measured cross sections are compared to theoretical calculations.

PACS numbers: 12.38.Qk,13.85.Ni,13.25.Ft,14.40.Lb

Measurements of heavy flavor production in $p\bar{p}$ collisions provide an opportunity to test predictions based on Quantum Chromodynamics (QCD). Previous measurements of B meson production cross sections in $p\bar{p}$ collisions at $\sqrt{s} = 1.8$ TeV were significantly larger than

Next-to-Leading-Order (NLO) QCD predictions [1, 2], although recent calculations with a more accurate description of b quark fragmentation have reduced this discrepancy [3, 4]. A measurement of charm meson production cross sections may help to understand this disagreement. In addition, there are no previous measurements using $p\bar{p}$ collisions. The upgraded Collider Detector at Fermilab (CDF II) has a new capability to trigger on displaced tracks from the decay of long-lived hadrons containing heavy flavor. We report here measurements of prompt charm meson cross sections using data recorded with this trigger in February and March 2002, corresponding to $5.8 \pm 0.3 \text{ pb}^{-1}$ of integrated luminosity.

An overview of the CDF II detector can be found elsewhere [5], only the components relevant to this analysis are described here. The CDF coordinate system has the z axis pointing along the proton momentum; φ is the azimuth, θ is the polar angle, and r is the distance from the proton beam axis. The CDF II central tracking region covers the pseudorapidity region $|\eta| \leq 1$, where $\eta = -\ln[\tan(\theta/2)]$. A superconducting solenoid provides a nearly uniform axial field of 1.4 T. The silicon vertex detector (SVX II) [6] consists of double-sided microstrip sensors arranged in five concentric cylindrical shells with radii between 2.5 and 10.6 cm. Surrounding the SVX II is the Central Outer Tracker (COT) [7], an open cell drift chamber covering radii from 40 to 137 cm. The COT has 96 layers, organized in 8 superlayers, alternating between axial and $\pm 2^\circ$ stereo readout.

CDF II has a three-level trigger system. We describe here the trigger used in this analysis. At the first trigger level, charged tracks are reconstructed in the COT axial projection by a hardware processor (XFT) [8]. The trigger for hadronic charm decays requires two oppositely charged tracks with $p_T \geq 2 \text{ GeV}/c$ and the scalar sum of the p_T 's larger than $5.5 \text{ GeV}/c$, where p_T is the magnitude of the component of the momentum transverse to the beam axis. At the second trigger level, the Silicon Vertex Tracker (SVT) [9] associates axial SVX II strip clusters from four layers with XFT track information. The SVT measures the distance of closest approach of a track relative to the beam axis (impact parameter or d_0) with a resolution of $50 \mu\text{m}$, which includes a contribution of $30 \mu\text{m}$ from the beam spot transverse size. Hadronic decays of heavy flavor are selected by requiring two tracks with $120 \mu\text{m} \leq d_0 \leq 1 \text{ mm}$ each. At the third trigger level, a farm of PCs performs complete event reconstruction online; the opening angle $\delta\varphi$ between the two trigger tracks is required to be between 2° and 90° , and the intersection point in the $r\text{-}\varphi$ plane projected along the net momentum vector of the two tracks must be more than $200 \mu\text{m}$ from the beamline.

We reconstruct charm mesons in the following decay modes: $D^0 \rightarrow K^-\pi^+$, $D^{*+} \rightarrow D^0\pi^+$ with $D^0 \rightarrow K^-\pi^+$, $D^+ \rightarrow K^-\pi^+\pi^+$, $D_s^+ \rightarrow \phi\pi^+$ with $\phi \rightarrow K^+K^-$, and their charge conjugates. For every track pair that satisfies the trigger requirements (trigger pair), we form one $D^0 \rightarrow K^-\pi^+$ candidate and a second candidate with the mass assignments swapped. No particle identification is used in this analysis. D^0 candidates within three standard deviations of the D^0 mass are combined with a third track with $p_T \geq 0.5 \text{ GeV}/c$ to form $D^{*+} \rightarrow D^0\pi^+$ candidates. The three-body decays of the D^+ and D_s^+ are reconstructed by combining a trigger pair with a third track having axial hits in at least three out of five SVXII layers and performing a vertex fit based on axial track information only. For D_s^+ reconstruction, we specifically require the $K^-\pi^+$ pair to satisfy the trigger requirements, since the typical opening angle between two kaons from ϕ decay is close to the $\delta\varphi \geq 2^\circ$ trigger requirement. Each ϕ candidate is required to have a mass within $\pm 20 \text{ MeV}$ of the world average ϕ mass. The D meson candidates are binned in p_T as indicated in Table I. The signals summed over all p_T bins are shown in Fig. 1.

The D^0 yield is obtained from a binned maximum likelihood fit to the $K^-\pi^+$ invariant mass distribution, with a narrow Gaussian for the D^0 signal, a linear function for the combinatoric background and a wide Gaussian describing $D^0 \rightarrow K^-\pi^+$ with the wrong mass assignment. We determine the shape of the mass distribution resulting from the wrong mass assignment using D^0 from D^{*+} decay where the charge of the low-momentum pion determines the mass assignment of the D^0 decay products. The D^{*+} yield is extracted from the distribution of $\Delta m = m(K^-\pi^+\pi^+) - m(K^-\pi^+)$, the mass difference between the $K^-\pi^+\pi^+$ and the $K^-\pi^+$ combination. The signal is modeled with two Gaussians with equal means, and the background is characterized as $a\sqrt{\Delta m - m_\pi} \exp(b(\Delta m - m_\pi))$, where a and b are free parameters in the fit. The D^+ signal is described with two Gaussians and the background is described with a linear function. In the $\phi\pi^+$ mode, we model the invariant mass distribution as a linear background with two Gaussians, one corresponding to the D^+ and one to the D_s^+ . We find 36804 ± 409 $D^0 \rightarrow K^-\pi^+$, 5515 ± 85 $D^{*+} \rightarrow D^0\pi^+$, 28361 ± 294 $D^+ \rightarrow K^-\pi^+\pi^+$, and 851 ± 43 $D_s^+ \rightarrow \phi\pi^+$, where the uncertainties quoted are statistical only. We vary the signal and background models and attribute systematic uncertainties on the signal yield in the range of $1\% - 6\%$, depending on the decay mode and the p_T range of the candidates.

We separate charm directly produced in $p\bar{p}$ interactions (prompt charm) from charm

from B decay (secondary charm) using the impact parameter of the net momentum vector of the charm candidate to the beamline [10]. Prompt charm mesons point to the beamline. The shape of the impact parameter distribution of secondary charm is obtained from a generator-level NLO Monte Carlo (MC) simulation of B meson production and decay. Both components are smeared with a resolution function (Gaussian + exponential tails) obtained from a sample of $K_S^0 \rightarrow \pi^+\pi^-$ decays that satisfy the trigger requirements. The impact parameter distribution of the reconstructed charm samples, shown for the D^0 in Fig. 2, is fit to a prompt and a secondary component. The prompt fraction is measured for each p_T bin. Averaged over all p_T bins, $(86.6 \pm 0.4)\%$ of the D^0 mesons, $(88.1 \pm 1.1)\%$ of D^{*+} , $(89.1 \pm 0.4)\%$ of D^+ , and $(77.3 \pm 3.8)\%$ of D_s^+ are promptly produced (statistical uncertainties only). The systematic uncertainties on the prompt fractions are estimated by removing the non-Gaussian tail in the resolution function and evaluating the variation. The relative uncertainty is found to be in the 3% – 4% range, depending on the decay mode.

Using a hit-level simulation of the COT, overlaid with data events to reproduce a realistic occupancy, we measure a reconstruction efficiency in the COT of 99% for tracks with $p_T \geq 2 \text{ GeV}/c$, falling to 95% at $p_T = 0.5 \text{ GeV}/c$. The efficiency for finding three SVXII axial hits on a reconstructed track is measured from data to be about 85%. The efficiencies of the trigger hardware XFT and SVT to reconstruct tracks are measured from data samples without XFT or SVT requirements [10]. The XFT tracking efficiency is greater than 95%. In the data-taking period considered, the SVXII and the SVT were not yet fully operational, and the efficiency varied as certain SVXII modules were included or excluded from the trigger. Therefore, we measured the SVT efficiency in 42 periods, each corresponding to one $p\bar{p}$ store of the Tevatron, and characterized the efficiency as a function of the track azimuth φ , the longitudinal position z_0 , the polar angle θ and the transverse momentum p_T . The average single-track efficiency of the SVT for this early data taking period was about 42%.

The measured efficiencies are applied to a generator-level NLO MC simulation of charm meson production and decay to calculate the trigger and reconstruction efficiencies, taking into account decay in flight and hadronic interactions of the charm meson decay products. The MC p_T spectrum of the charm mesons is reweighted to match the measured p_T spectrum. The integrated cross section σ_i in each p_T bin i with $|y| \leq 1$ (where $y = \frac{1}{2} \ln(\frac{E+p_z}{E-p_z})$ and E

is the energy of the charm meson) is calculated using the following equation:

$$\sigma_i = \frac{N_i/2 \cdot f_{D,i}}{\int \mathcal{L} dt \cdot \epsilon_i \cdot \mathcal{B}}, \quad (1)$$

where N_i is the number of charm mesons in each p_T bin and $f_{D,i}$ is the fraction of prompt charm in that bin. The integrated luminosity $\int \mathcal{L} dt$ is based on an inelastic cross section $\sigma_{pp} = 60.7 \pm 2.4 \text{ mb}$ and has a total uncertainty of 6%. The factor $\frac{1}{2}$ is included because we count both D and \bar{D} mesons, but we report cross sections for D alone. We verified that the D and \bar{D} cross sections are equal within statistical uncertainties. The branching fractions \mathcal{B} are taken from Ref. [11]. For the D^0 cross section, we sum the branching fractions of $D^0 \rightarrow K^- \pi^+$ and $D^0 \rightarrow K^+ \pi^-$, since both contribute to the observed signal. The combined reconstruction and trigger efficiency ϵ_i varies from 0.12% to 1.9% depending on the decay mode and the p_T bin. Systematic uncertainties on the trigger and reconstruction efficiency arise predominantly from the uncertainty on single-track efficiencies and two-track efficiency correlations. They also have contributions from ionization energy loss, hadronic interactions in the inner tracker material and the size of the interaction region. The combined systematic uncertainty on the trigger and reconstruction efficiency is in the range of 8%–14%, depending on the decay mode and the p_T range of the D mesons.

The total cross sections are obtained by summing over all p_T bins. However, the last p_T bin is replaced by an inclusive bin with $p_T > 12 \text{ GeV}/c$. We find $\sigma(D^0, p_T \geq 5.5 \text{ GeV}/c) = 13.3 \pm 0.2 \pm 1.5 \mu\text{b}$, $\sigma(D^{*+}, p_T \geq 6.0 \text{ GeV}/c) = 5.2 \pm 0.1 \pm 0.8 \mu\text{b}$, $\sigma(D^+, p_T \geq 6.0 \text{ GeV}/c) = 4.3 \pm 0.1 \pm 0.7 \mu\text{b}$ and $\sigma(D_s^+, p_T \geq 8.0 \text{ GeV}/c) = 0.75 \pm 0.05 \pm 0.22 \mu\text{b}$, where the first uncertainty is statistical and the second systematic. To calculate the differential cross sections, we divide σ_i by the width of the p_T bin. Since we report $d\sigma/dp_T$ at the center of each p_T bin, we apply a correction to account for the non-linear shape of the cross section. The results are listed in Table I.

The measured differential cross sections are compared to two recent calculations [12, 13], as shown in Fig. 3. The uncertainties on the calculated cross sections are evaluated by varying independently the renormalization and factorization scales between 0.5 and 2 times the default value. Contributions from other sources, such as the charm quark mass, the value of the strong coupling constant and the fragmentation functions, were reported to be smaller and are not taken into account. The measured differential cross sections are higher than the theoretical predictions by about 100% at low p_T and 50% at high p_T . However,

they are compatible within uncertainties. The same models also underestimate B meson production at $\sqrt{s} = 1.8$ TeV by similar factors [2–4].

We thank the Fermilab staff and the technical staffs of the participating institutions for their vital contributions. This work was supported by the U.S. Department of Energy and National Science Foundation; the Italian Istituto Nazionale di Fisica Nucleare; the Ministry of Education, Culture, Sports, Science and Technology of Japan; the Natural Sciences and Engineering Research Council of Canada; the National Science Council of the Republic of China; the Swiss National Science Foundation; the A.P. Sloan Foundation; the Bundesministerium fuer Bildung und Forschung, Germany; the Korean Science and Engineering Foundation and the Korean Research Foundation; the Particle Physics and Astronomy Research Council and the Royal Society, UK; the Russian Foundation for Basic Research; and the Comision Interministerial de Ciencia y Tecnologia, Spain;

- [1] B. Abbott *et al.* [D0 Collaboration], Phys. Lett. B **487**, 264 (2000).
- [2] D. Acosta *et al.* [CDF Collaboration], Phys. Rev. D **65**, 052005 (2002).
- [3] M. Cacciari and P. Nason, Phys. Rev. Lett. **89**, 122003 (2002).
- [4] J. Binnewies, B. A. Kniehl and G. Kramer, Phys. Rev. D **58**, 034016 (1998).
- [5] R. Blair *et al.* [CDF-II Collaboration], FERMILAB-PUB-96-390-E.
- [6] A. Sill [CDF Collaboration], Nucl. Instrum. Meth. A **447**, 1 (2000).
- [7] K. T. Pitts [CDF Collaboration], Nucl. Phys. Proc. Suppl. **61B**, 230 (1998).
- [8] E. J. Thomson *et al.*, IEEE Trans. Nucl. Sci. **49**, 1063 (2002).
- [9] W. Ashmanskas *et al.*, Nucl. Instrum. Meth. A **447**, 218 (2000).
- [10] C. Chen, Ph.D. thesis, University of Pennsylvania, 2003.
- [11] K. Hagiwara *et al.* [Particle Data Group Collaboration], Phys. Rev. D **66**, 010001 (2002).
- [12] M. Cacciari and P. Nason, arXiv:hep-ph/0306212.
- [13] Private communication, B.A. Kniehl. Their calculation employs the method described in
B.A. Kniehl, G. Kramer, B. Potter, Nucl.Phys.**B597**, 337-369 (2001)

		$d\sigma(y \leq 1)/dp_T$ [nb/(GeV/c)]			
p_T range	Central p_T	D^0	D^{*+}	D^+	D_s^+
[GeV/c]	[GeV/c]				
5.5 – 6	5.75	$7837 \pm 220 \pm 884$	—	—	—
6 – 7	6.5	$4056 \pm 93 \pm 441$	$2421 \pm 108 \pm 424$	$1961 \pm 69 \pm 332$	—
7 – 8	7.5	$2052 \pm 58 \pm 227$	$1147 \pm 48 \pm 145$	$986 \pm 28 \pm 156$	—
8 – 10	9.0	$890 \pm 25 \pm 107$	$427 \pm 16 \pm 54$	$375 \pm 9 \pm 62$	$236 \pm 20 \pm 67$
10 – 12	11.0	$327 \pm 15 \pm 41$	$148 \pm 8 \pm 18$	$136 \pm 4 \pm 24$	$64 \pm 9 \pm 19$
12 – 20	16.0	$39.9 \pm 2.3 \pm 5.3$	$23.8 \pm 1.3 \pm 3.2$	$19.0 \pm 0.6 \pm 3.2$	$9.0 \pm 1.2 \pm 2.7$

TABLE I: Summary of the measured prompt charm meson differential cross sections and their uncertainties at the center of each p_T bin. The cross sections are reported only for bins of p_T with large enough acceptance to allow reliable determination of the cross section. The first error is statistical and the second systematic. The products of the branching fractions [11] used are $(3.81 \pm 0.09)\%$, $(2.57 \pm 0.06)\%$, $(9.1 \pm 0.6)\%$ and $(1.8 \pm 0.5)\%$ for D^0 , D^{*+} , D^+ and D_s^+ , respectively.

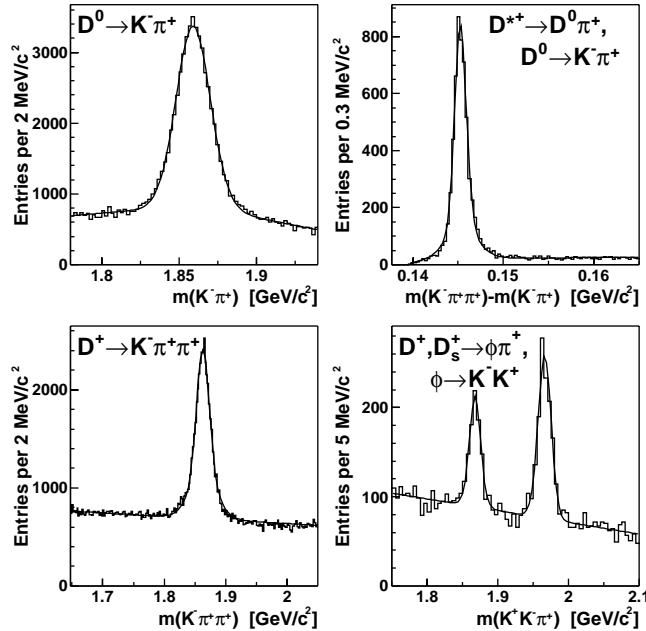


FIG. 1: The invariant mass distributions for the four charm meson species. The curves are the sum of the fit results from the individual p_T bins.

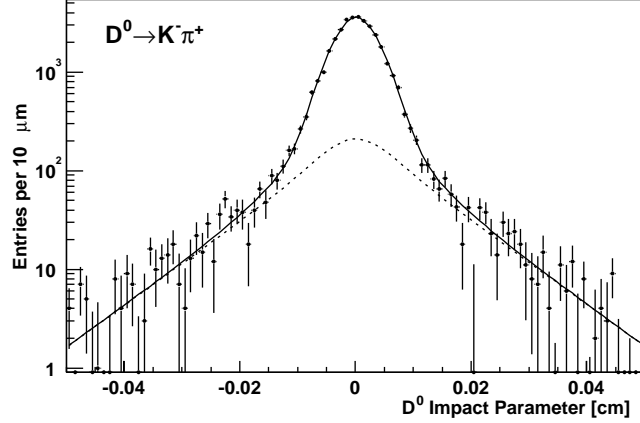


FIG. 2: The impact parameter distributions of the D^0 mesons, measured from the $\pm 2\sigma$ signal region of the invariant mass distribution and corrected for combinatoric background measured in the invariant mass sidebands. The solid curve is the fit result summed over all p_T bins. The dashed curve shows the contribution of secondary charm from B decay.

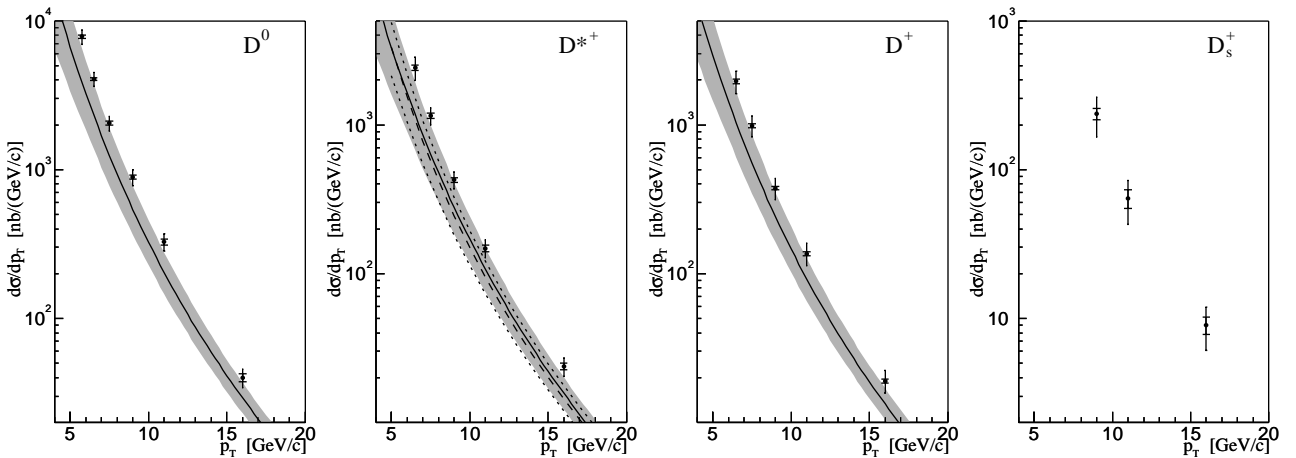


FIG. 3: The differential cross section measurements for $|y| \leq 1$. The inner bars represent the statistical uncertainties; the outer bars are the quadratic sums of the statistical and systematic uncertainties. The solid curves are the theoretical predictions from Cacciari and Nason [12], with the uncertainties indicated by the shaded bands. The dashed curve shown with the D^{*+} cross section is the theoretical prediction from Kniehl [13]; the dotted lines indicate the uncertainty. No prediction is available yet for D_s^+ production.